High-Efficiency Distributed Phase Plate Generation and Characterization

An essential requirement for both direct-drive and indirect-drive laser fusion is the uniform irradiation of targets that are located at the far field and quasi far field of the laser system. Higher uniformity results in reduced Rayleigh-Taylor instabilities and improved spherical convergence of fuel capsules during high-density compression. For high-power, solid-state laser drivers, a major contribution to irradiation nonuniformity is the intensity distribution of the individual frequency-tripled beams at the target plane. The irradiance nonuniformities are caused primarily by spatial variations in the near-field phase front that accumulate as the pulse propagates through the air and laser optics. Optical phase conversion at the end of a laser system, using distributed phase plates (DPP's),[1] modifies the beam's field coherence, thereby changing its focusing properties and shifting energy toward the higher spatial frequencies that can be rapidly blurred using temporal beam-smoothing techniques.

In the past, the price of this coherence control was a loss of 20%–25% of the laser energy. The primary goal in the design of a new phase converter is to achieve lossless, wavefront-insensitive, phase conversion. This has been recently achieved with a new variety of DPP (continuous, deep-surface-relief phase plates) that has been generated and characterized for use in the 60-beam OMEGA laser system. The two-level binary phase plates previously deployed on the 24-beam OMEGA laser system provided coherence control but had significant losses and operated over a narrow range in the focal direction. These new continuous DPP's perform nearly lossless phase conversion of high-power laser beams,[2,3] providing a coupling efficiency to target of $\gtrsim$95%. They also operate over the full range of target diameters planned for the LLE experimental fusion-physics program.

OMEGA DPP Requirements

The requirements for this new generation of DPP's are high transmission to the target, a weak super-Gaussian irradiance profile, and operation over a range of target sizes. They must be significantly more efficient than the previous two-level DPP's whose overall coupling efficiency was limited to 78%. Of that lost energy (22%), 16% was due to diffraction rings produced by the edges of the binary elements. The goal was to retrieve all of this energy by implementing continuous features on the phase plates, thereby eliminating the diffraction loss. This would result in DPP's that have to-target transmission efficiencies of 94%–96%. The DPP design should provide an intrinsic efficiency of 100%; however, some loss is allowed to accommodate both alignment and manufacturing tolerances. Of the remaining 4% to 6% energy loss, approximately 3.5% must be allocated to beam-to-target alignment tolerances. Therefore, additional energy losses associated with the manufacturing process, such as surface scatter and reflection, must be limited to less than 2.5% of the incident energy.

The required irradiance envelope produced by the DPP's is mathematically represented by a rotationally symmetric supergaussian of order between 2 and 3. (An order 2 produces a Gaussian distribution.) It is also desired that the DPP provide the relatively flat power spectrum characteristic of the previous two-level DPP's. When these distributions are overlapped on a target, the amplitudes of the low- to mid-range modes ($\lambda > 20\ \mu$m) should not exceed the extremes produced by random statistics. High spatial frequencies ($\lambda < 20\ \mu$m) are less detrimental because of their fast smoothing times in the presence of temporal beam smoothing.

The DPP must also provide an irradiance distribution that adequately integrates over the full aperture of the input pupil so that the spectral modes, produced by spatial color cycling, overlap at the target plane. DPP's containing Fourier gratings inherently meet this requirement when used at or near the focal plane of a lens. Finally, the new DPP must provide the above efficiency, irradiance, power spectrum, and temporal beam-smoothing capability for target diameters ranging from 800 to 1000 μm. On OMEGA this necessitates operation in a range of ±4 mm along the optical axis of the lens.

Phase-Plate Concept

To achieve both high efficiency and the desired profile at the target plane, the continuous DPP was designed with a

specific combination of a Fourier grating phase plus a random phase. Produced by the surface relief on such a DPP, the phase consists of a random term combined with several spatially periodic terms. These two terms are superposed on a single surface but are shown in Fig. 65.1 on either side of a plate for clarity only. The purpose of the spatially periodic terms, or Fourier grating terms, is to diffract the collimated incident beam into multiple orders or multiple beamlets.[2] These orders are collected by the lens to form an array of foci at the Fourier plane of the lens. The lateral separation of these foci (d^*) can be expressed in terms of the wavelength λ of light used, the f number ($f_{\#}$) of the focusing lens, and the number of grooves or elements in the grating, N:

$$d^* = \lambda N f_{\#} = \frac{\lambda N f}{D} = \frac{\lambda f}{d}, \tag{1}$$

where N is equal to the diameter of the grating (D) divided by the groove spacing (d); $N = D/d$. The Fourier gratings separate an incident laser beam into a two-dimensional angular spectrum of beamlets that focus at the focal plane of a lens. As a result, the interference pattern produced by the coherent overlap of the beamlets depends primarily on the phase transfer function of the distributed phase plate rather than the wavefront of a typical laser beam.

In the simplest case, the surface-relief profile of a DPP can be composed of several sinusoidal components together with a random component. The phase retardation is distributed over the DPP surface by introducing optical path differences (OPD's) in the form of a thin film of varying thickness $t(x,y)$ and material refractive index n. The exact amount of phase retardation ϕ experienced by a transmitted wavefront depends upon the wavelength (λ) of light and is given by

$$\phi = \frac{2\pi}{\lambda}(\mathrm{OPD}) = \frac{2\pi}{\lambda}\left[t(x,y)(n-1)\right]. \tag{2}$$

Optical modeling shows that the energy coupled to a target using the new continuous distributed phase plate is substantially greater than that using a two-level binary phase plate as shown in Fig. 65.2. To allow for small beam and target misalignments, approximately 3.5% of the incident energy misses the target. This energy is accessible with the penalty of lower irradiation uniformity. Underfilling a spherical target causes an increase in the amplitude of medium-order spherical harmonic modes. Nevertheless, an increase in energy efficiency from 78% to 96% represents a 20%–25% increase in total energy delivered to the target. Simulations have shown that phase conversion with our new continuous DPP's meets the design requirements over a sufficiently long depth of focus to accommodate a wide range of target diameters.

DPP Generation

Optical lithography is an excellent means of generating complex surface-relief structures that subsequently can be replicated into polymers that are compatible with high-irradiance UV laser light. Using a combination of photographic and photolithographic techniques, both mask fabrication and photoresist patterning have been successfully demonstrated at

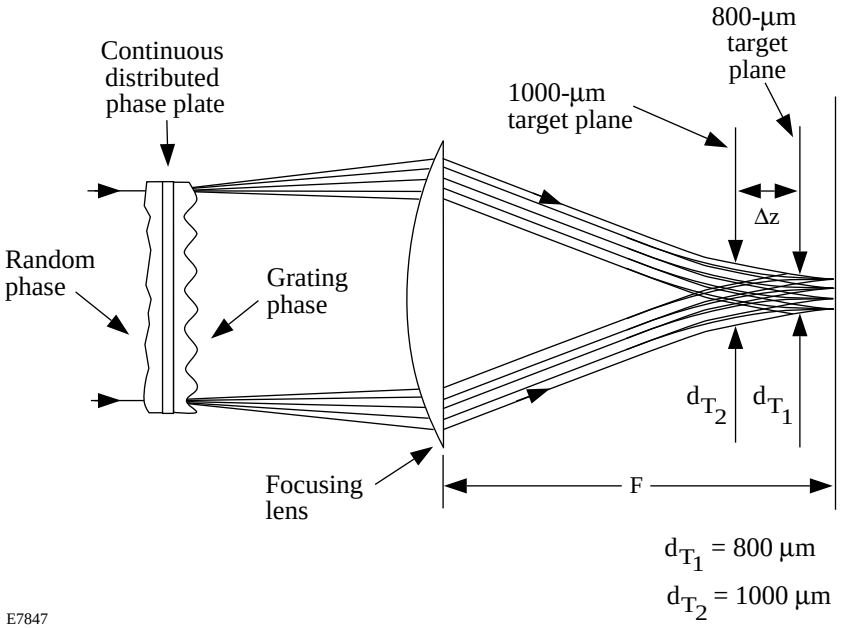

E7847

Figure 65.1
The surface of a continuous distributed phase plate consists of a random term combined with several periodic terms. These produce an irradiance distribution at the focal plane of a lens that efficiently couples laser light to targets in the range of 800 to 1000 μm in diameter. The two phase terms are shown on either side of the substrate for clarity only.

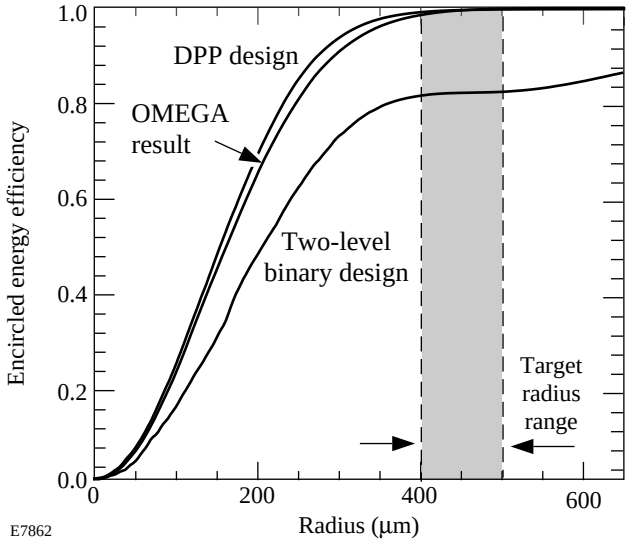

Figure 65.2
The energy coupled to a target using a continuous distributed phase plate is substantially greater than that using a two-level binary phase plate. Approximately 4% of the incident energy is distributed around the target to allow for minor beam and target misalignments. An increase in energy efficiency from 78% to 96% represents a 20%–25% increase in total energy delivered to the target.

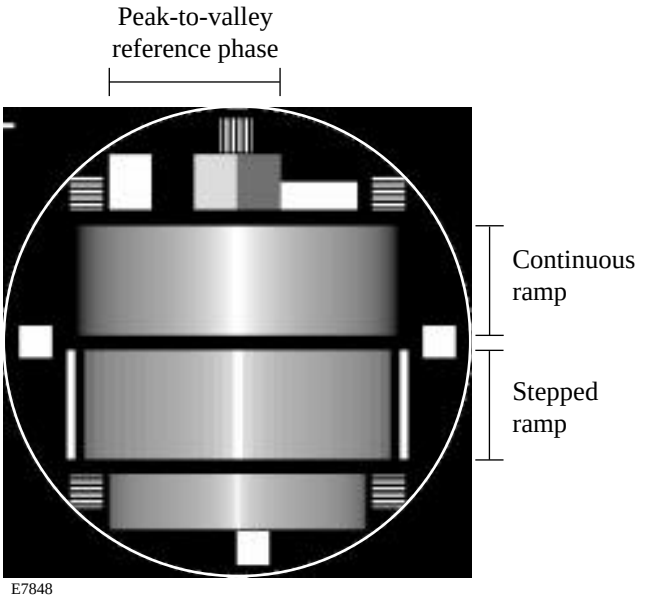

Figure 65.3
The calibration mask is a sheet of photographic film containing both continuous and stepped regions of varying density whose corresponding transmittance functions are used to characterize the linearity of the photolithographic process. A 9-in. enlargement made from a computer-generated, 35-mm negative is produced using standard silver-halide processing techniques.

LLE, resulting in the fabrication of 310-mm-diam continuous DPP's suitable for use in OMEGA.

The photolithographic process begins with the calibration of a Celco photographic-film writer, using, as a reference, the interferometric measurement of a test phase plate made in photoresist. The calibration mask used in this stage is a sheet of photographic film containing both continuous and stepped regions of varying density whose transmittance functions are used to characterize the linearity of the photolithographic process. An enlargement made from a computer-generated, 35-mm negative, shown in Fig. 65.3, is produced using standard silver-halide processing techniques. Following the chemical processing of the photoresist, Fizeau interferometry is used to characterize the optical path differences within the photoresist phase plate. The interference fringes, shown in Fig. 65.4, are computer analyzed to examine linearity of the transfer from mask transmittance to phase difference in the photoresist. These results are used to generate an end-to-end process inversion curve.

The final inversion curve, shown in Fig. 65.5, relates the Celco film writer's code values to the range of phase differences required in the DPP design. The inversions contained in

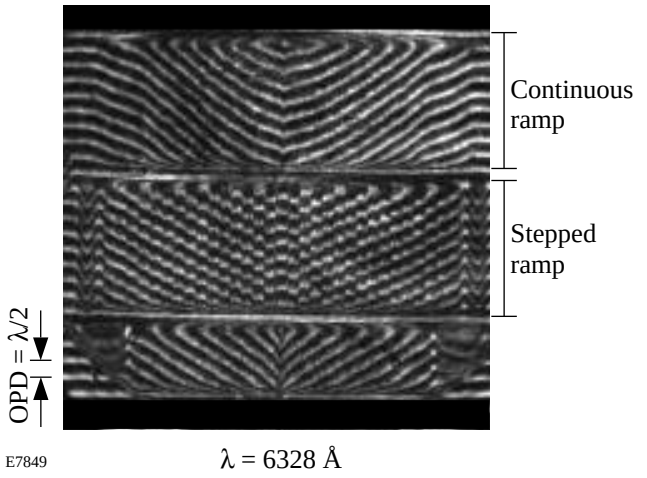

Figure 65.4
Fizeau interferometry is used to characterize the optical path differences that are photolithographically generated in a photoresist coating using the calibration mask shown in Fig. 65.3. The interference fringes are computer analyzed to examine linearity of the transfer from mask transmittance to photoresist phase difference.

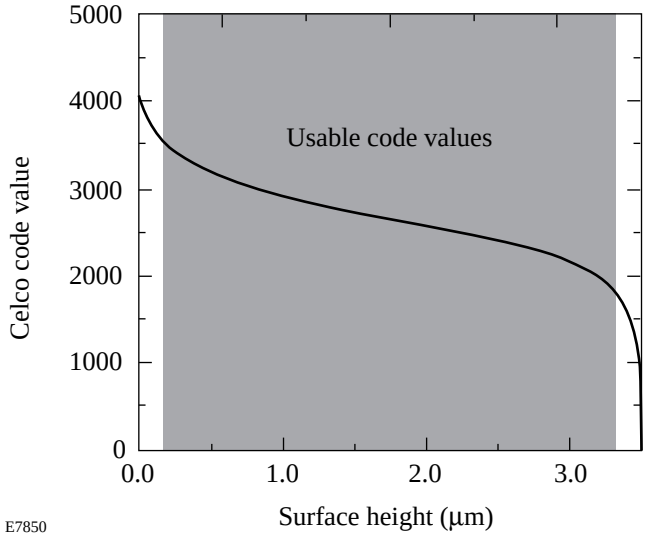

Figure 65.5
The final inversion curve relates the code values for the Celco film writer to the range of phase differences required in the DPP design. The multiple inversions contained in this final curve include nonlinearities in the film writer, recording film, enlargement film, and photoresist. Several iterations were required to yield a sufficiently linear relationship between the desired phase differences and the actual phase difference realized in the surface relief of the photoresist.

this final curve include the nonlinearities in the film writer, recording film, enlargement film, and photoresist. Several iterations were required to yield a sufficiently linear relationship between the desired phase differences and those produced in the surface relief of the photoresist. The mask used to generate the desired DPP surface relief is shown in Fig. 65.6. It is a sheet of silver halide film containing the distribution of densities that follow the range established by the previous calibration process. The mask transmittance function times the material removal function of the photoresist is linearly related to the phase difference produced in the DPP design.

Interferometric analysis of the DPP master is performed by positioning the edge of the master in a single-pass Mach-Zehnder interferometer. Spatial synchronous phase detection is used to analyze the high-frequency fringes that extend from the region of thick photoresist to the region of thin photoresist. Low-frequency fringes are shown in Fig. 65.7(a) to help the reader visualize the phase shifts. The peak-to-valley optical path difference, shown in Fig. 65.7(b), corresponds to the maximum phase difference contained in the photoresist DPP master.

The final steps to generate DPP's for the OMEGA laser system involves the transfer, or replication, of the surface relief into a suitable UV-compatible material. After extensive development of release mechanisms, the replication of photoresist

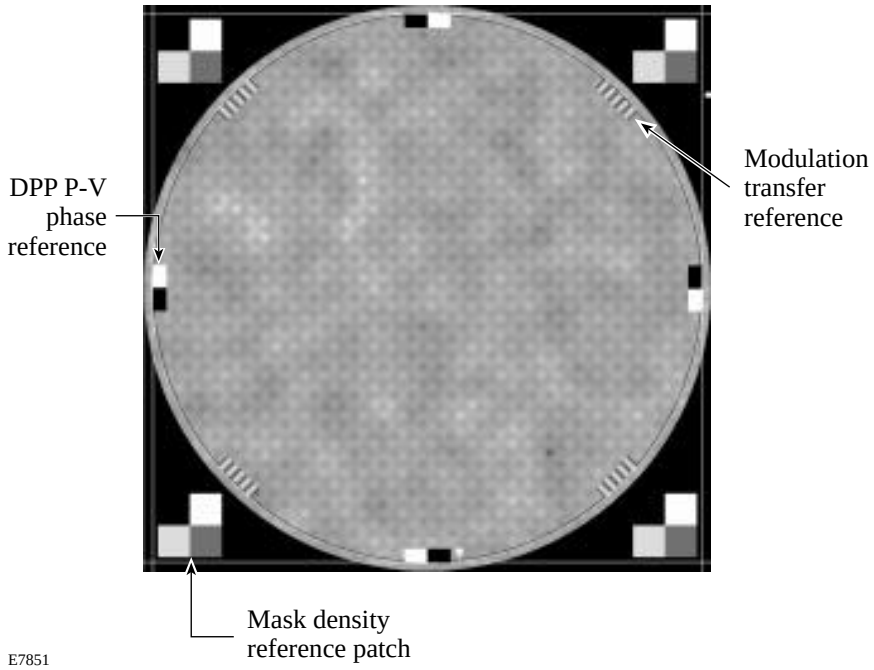

Figure 65.6
The mask used to generate the desired DPP surface relief is a sheet of photographic silver halide film containing a density distribution whose transmittance function follows the range established by the previous calibration iteration. The mask transmittance function times the material removal function of the photoresist is linearly related to the phase difference required in the DPP design.

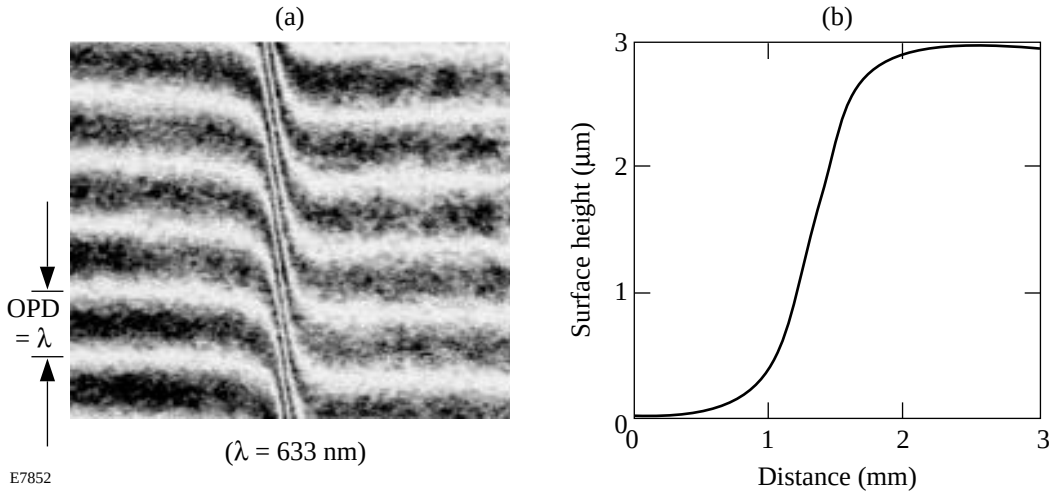

Figure 65.7
Interferometric analysis of the DPP master is performed by positioning the edge of the master within a single-pass Mach-Zehnder interferometer. Spatial synchronous phase detection is used to analyze the high-frequency interference fringes that extend from the region of thick photoresist to the region of thin photoresist. Low-frequency fringes are shown in (a) for clarity. The peak-to-valley optical path difference (b) measured here corresponds to the maximum phase difference contained in the DPP phase distribution.

masters into a UV epoxy succeeded using an evaporative-coating release-layer technology borrowed from the industrial sector.[4] The fabrication of DPP's is performed in class 100 to 1000 clean-room conditions to limit contamination that can cause losses due to surface-relief scattering, material scattering, and material absorption.

DPP Characterization

The on-target irradiation distribution from a single focused laser beam is measured with equivalent-target-plane photographic cameras. Experimental results from these cameras are shown in Fig. 65.8. Each element within the array represents the same spatial image recorded at successively lower exposures. Figure 65.8(a) shows a focal-spot distribution produced by a two-level binary phase plate, while Fig. 65.8(b) shows the more efficient pattern produced by the new continuous DPP. Note that the diffraction lobes are absent from the spot produced by the continuous DPP. These images were density-to-irradiance converted using a calibration curve derived from the known changes in exposure between images of each array. As can be seen in Fig. 65.9, a dynamic range of 10^4 is then obtained. This range is required to accurately measure the high-contrast speckle produced by phase conversion of the laser beam.

A photographic image generated with cw laser light [Fig. 65.10(a)] is compared with that from a beamline of the OMEGA laser system [Fig. 65.10(b)]. Although the wavelength of the cw (364-nm) laser is different than the OMEGA laser (351 nm), compensating diffractive and refractive effects

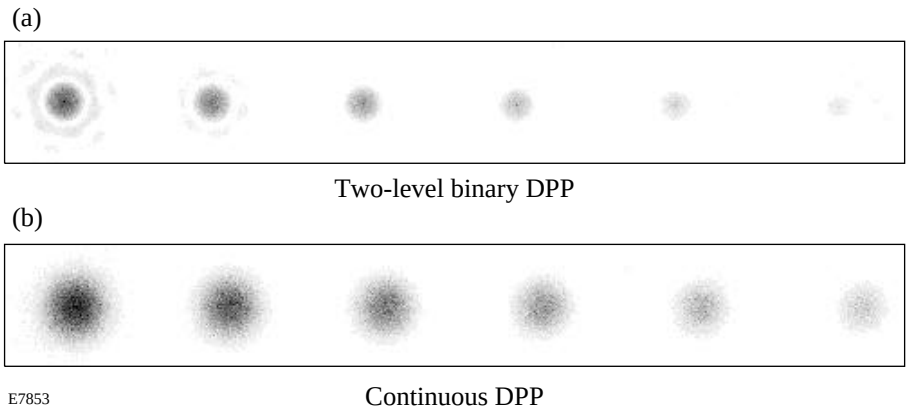

Figure 65.8
The on-target irradiation distribution from a single focused laser beam is measured with an equivalent-target-plane photographic camera. Each element within the array represents the same spatial image recorded at successively lower exposures. Figure 65.8(a) shows the lossy diffraction lobes produced by a two-level binary phase plate, while Fig. 65.8(b) shows the more efficient pattern produced by the new continuous DPP.

cause these results to be essentially equivalent. Orthogonal scans through the center of an equivalent-target-plane image show the irradiance modulation that is characteristic of laser speckle. The dominant visual characteristic for these phase plates is the random variation in irradiance, which obeys negative exponential statistics. Figures 65.11(a) and 65.11(b) show horizontal and vertical cross sections of the irradiance, respectively, for the OMEGA beam shown in Fig. 65.10(b). An individual cross section can contain a peak-to-average irradiance ratio of several hundred percent; however, only a small fraction of the total energy resides in these modulations. Figure 65.12 shows the total energy contained within a circle surrounding the center of the beam as a function of the radius of that circle. This is referred to as an encircled energy plot. Curve A is an experimental cw result, curve B is an experimental pulsed result, curve C is the result of theoretical calculation, and curve D is the desired encircled energy profile for the irradiation for direct-drive targets. Good agreement between these curves, near the 400-μm radius, indicates that a useful, highly efficient DPP has been generated.

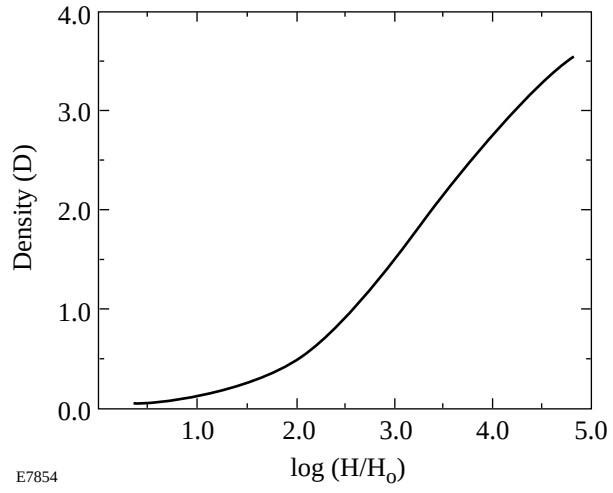

Figure 65.9
The photographic images generated by the equivalent-target-plane camera are density-to-irradiance converted using a calibration curve derived from the array of images. A dynamic range of 10^4 is obtained to accurately measure the high-contrast speckle produced by phase conversion of the laser beam.

Extensive testing of the DPP far-field performance is performed to ensure that accurate focusing can be accomplished on the OMEGA laser system. In addition to the photographic analysis described above, energy-transfer measurements are made by translating target-sized apertures along the optical axis. These measurements are used to determine both the minimum spot size and the energy-transfer efficiency of the DPP. Equation (3) shows the functional form of the relationship between target diameter and focal shift for a given DPP-specific minimum spot and a desired encircled energy on target:

$$\Delta Z_T = 6.429\left(D_m\right)\left[\left(\frac{D_T}{D_m}\right)^{N\left(E_c\right)} - 1\right]^{1/N\left(E_c\right)} + \Delta Z_p \ , \quad (3)$$

where D_m = minimum beam diameter containing E_c; D_T = target diameter (800 to 1000 μm); E_c = encircled energy on target; $N(E_c)$ = calculated order; and ΔZ_p = power-induced focal shift. The minimum spot size (D_m) is used in Eq. (3) to provide the correct position of the focus lens given a desired target diameter and a specific encircled energy. A limited amount of defocus can be used to compensate for DPP

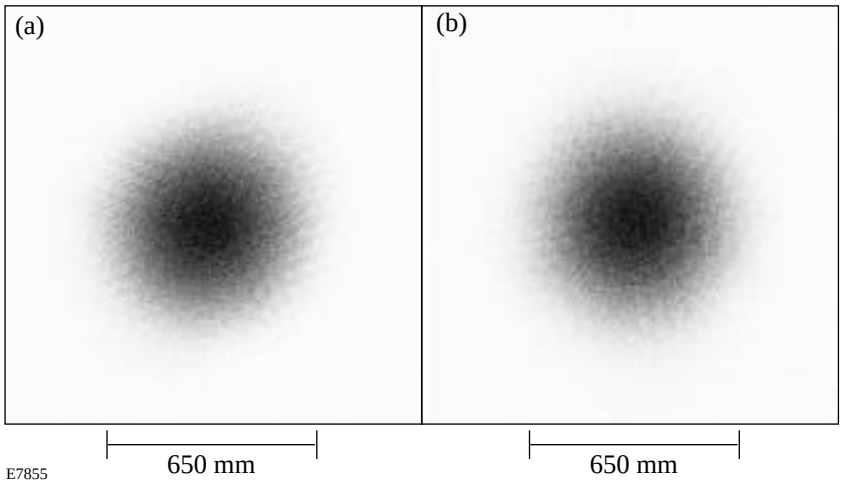

Figure 65.10
(a) The photographic image generated with cw laser light is compared with (b) that from a beamline of the OMEGA laser system. Although the wavelength of the cw (364-nm) laser is different than the 351-nm OMEGA laser, compensating diffractive and refractive effects cause these results to be essentially equivalent.

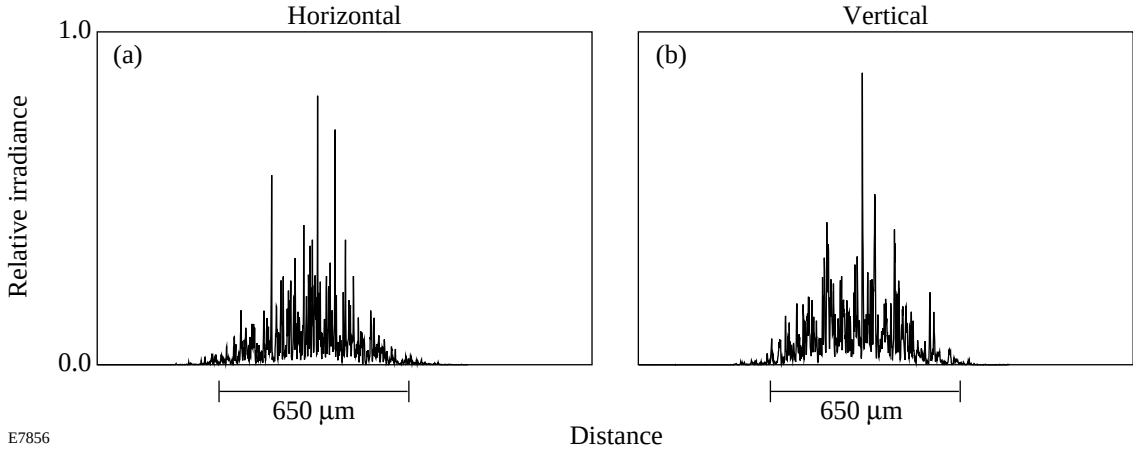

Figure 65.11
Orthogonal scans through the center of an equivalent-target-plane image show the irradiance modulation characteristic of laser speckle. Figures 65.11(a) and 65.11(b) show horizontal and vertical cross sections of the irradiance, respectively. An individual cross section can contain a peak-to-average irradiance ratio of several hundred percent; however, only a small fraction of the total energy is contained in these peaks.

phase undermodulation, thus providing a favorable manufacturing tolerance.

The family of hyperbolic curves shown in Fig. 65.13 represent a specific case of Eq. (3). The radius of the contour containing 96.6% of the energy is plotted as a function of the focus lens position along the optical axis. Minimum spot sizes of between 675 and 750 μm are represented here. The gradient of the curve in the vicinity of an 800-μm target is approximately a change in diameter of 10 μm per 100 μm of focal shift. Additional families of hyperbolic curves can be generated to allow flexibility in choosing an encircled energy on target; the limits, however, are the amount of energy that misses the target and the overall irradiation uniformity. A coupling efficiency of 96.6% (incident light that irradiates the target) is a compromise between these constraints.

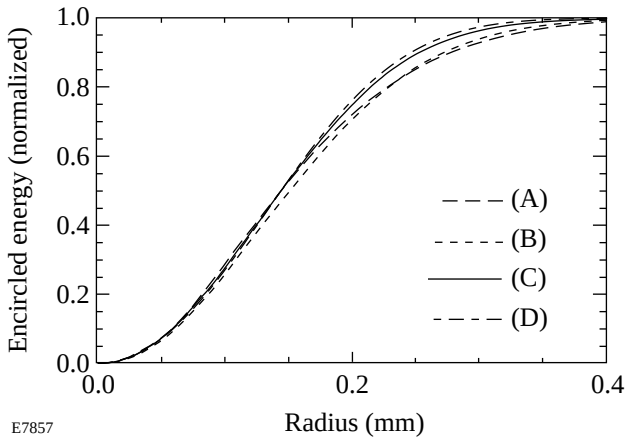

Figure 65.12
The total energy contained within a circle surrounding the center of the beam is plotted as a function of the radius of the circle. Curve A is an experimental cw result, curve B is an experimental pulsed result, curve C is the result of theoretical calculation, and curve D is the desired encircled energy profile.

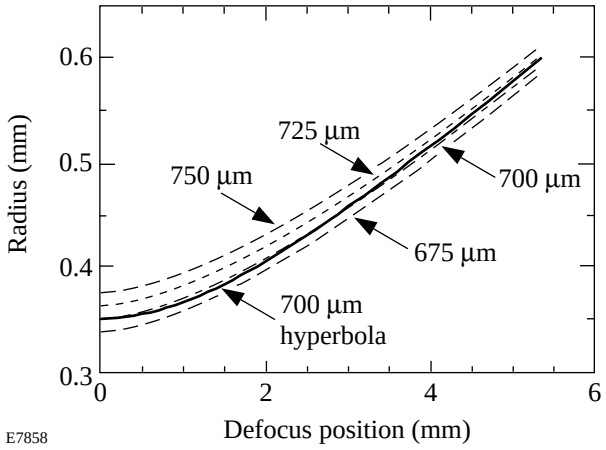

Figure 65.13
The radius of the contour containing 96.6% of the energy presented to the focal plane is plotted as a function of the shift of the focus lens along the optical axis. A range of target diameters between 800 and 1000 μm can be irradiated with the new continuous DPP. The gradient of the curve in the vicinity of an 800-μm target is approximately a change in diameter of 10 μm per 100 μm of focal shift.

Conclusions

An extensive development program has produced significantly improved DPP's that are characterized as continuous, deep-surface-relief phase plates. These DPP's can perform nearly lossless phase conversion of high-power UV laser beams, thus delivering up to 25% more energy than previous designs. These DPP's also provide the desired irradiance envelope and speckle distribution over the full 800- to 1000-μm range of target diameters envisioned for the near-term experimental target physics program at LLE. In addition, epoxy-replicated DPP's exhibit high damage thresholds and meet the design requirements for the upgraded OMEGA laser system. It is anticipated that near-term target experiments will be carried out on OMEGA to study the hydrodynamic benefits of these new DPP's with temporal beam smoothing and that additional criteria will be established to design fully optimized DPP's for the future.[5,6]

ACKNOWLEDGMENT

This work was supported by the U.S. Department of Energy Office of Inertial Confinement Fusion under Cooperative Agreement No. DE-FC03-92SF19460, the University of Rochester, and the New York State Energy Research and Development Authority. The support of DOE does not constitute an endorsement by DOE of the views expressed in this article.

REFERENCES

1. Laboratory for Laser Energetics LLE Review **33**, NTIS document No. DOE/DP/40200-65, 1988 (unpublished), p. 1

2. T. J. Kessler, Y. Lin, J. JArmstrong, and B. Velazquez, in *Laser Coherence Control: Technology and Applications*, edited by H. T. Powell and T. J. Kessler (SPIE, Bellingham, WA, 1993), Vol. 1870, pp. 95–104.

3. Laboratory for Laser Energetics LLE Review **55**, NTIS document No. DOE/DP/40200-257, 1993 (unpublished), p. 146.

4. Opticon Replication Center, 799 Middlesex Turnpike, Billerica, MA 01821.

5. Y. Lin, T. J. Kessler, and G. N. Lawrence, Opt. Lett. **20**, 764 (1995).

6. Laboratory for Laser Energetics LLE Review **64**, NTIS document No. DOE/SF/19460-99, 1995 (unpublished), p. 170.